Technische Universität München
Fakultät für Physik

Abschlussarbeit im Bachelorstudiengang Physik

Untersuchung der Modellabhängigkeit der Partialwellenanalyse des Kππ-Endzustandes

Study of the Model Dependence of the Partial-Wave Analysis of the Kππ Final State

Julien Beckers

August 2018

Themensteller: Prof. S. Paul
Zweitgutachter: Prof. R. Diehl

Contents

Introduction

Hadrons are composite particles held together by the strong interaction. The most prominent hadrons are the proton and neutron. However, most hadrons are extremely short-lived resonances that can be produced e.g. in inelastic scattering experiments. Their spectrum is in parts only poorly known. Precision measurements in experiments with, e.g., light mesons, intend to increase the knowledge about the hadron spectrum and the behaviour of the strong interaction at low energies.

The COMPASS experiment at CERN is a such high-energy physics experiment. Using CERN's SPS accelerator, it aims to study the hadron spectrum of light mesons, which are composed of up, down or strange quarks. These mesons are produced in inelastic scattering reactions of a 190 GeV/c secondary hadron beam, which is produced by the 400 GeV/c SPS proton beam impinging on a beryllium target. The hadron beam, which consists mostly of π with a small admixture of K, is shot onto a liquid-hydrogen target. In the strong decay observed, the colliding particles form unstable intermediate, labelled X^-, that are assumed to be dominated by resonances. The goal of the COMPASS experiment is to identify and study these resonances through the final-state particles. For this analysis, the *partial-wave method* is employed. In order to be able to calculate the X^- decay amplitude, it is assumed that the decay takes place as a series of two-body decays, with additional intermediate two-body resonance states ξ, called the *isobars*. However, isobar parameters, i.e. the masses and widths of the isobar resonances, need to be known precisely from other experiments. For practical reasons, these parameters cannot be left as free parameters in the analysis, which leads to important systematic uncertainties.

In this thesis, we therefore investigate these uncertainties and study the parameters of some isobars that appear in the partial-wave analysis of the $K^-\pi^+\pi^-$ final state, using the maximum likelihood method. This method is used to compare a model to measured data, by construction of a likelihood value, which indicates how well the model fits to the data. We will search for those isobar parameters which yield the highest likelihood for four hadronic isobar resonances, and compare them to the world averages that are used in the partial-wave analysis.

Chapter 1

Methods

In this chapter, we will give a short overview of the analysis methods and formalisms used for the description of the studied scattering processes and the evaluation of the COMPASS data. A more mathematically in-depth description can be found in [1].

1.1 Partial-wave analysis

1.1.1 Scattering process

We study diffractive dissociation reactions of hadrons of the following form:

$$\underbrace{a}_{\text{high-energetic beam particle}} + \underbrace{b}_{\text{target particle}} \rightarrow \underbrace{(1+2+3)}_{\text{hadronic final state}} + \underbrace{c}_{\text{target recoil}} \tag{1.1}$$

More precisely, we examine the collision

$$K^- + p \rightarrow (K^- \pi^+ \pi^-) + p_{\text{recoil}} \tag{1.2}$$

of a kaon beam on a hydrogen target, illustrated in fig. 1.1a.

The basic assumptions of the analysis method are that the three-body intermediate states X^-, produced by the excitation of the K^- via the strong interaction, are dominated by resonances, so that the scattering process can be decomposed into two independent reactions:

$$K^- + p \rightarrow X^- + p_{\text{recoil}} \quad \text{and} \quad X^- \rightarrow K^- \pi^+ \pi^-$$

Resonance production and decay are independent and can be treated separately. Therefore, we can factorize the amplitude $\mathcal{M}_{f,i}$ describing a certain state X into a
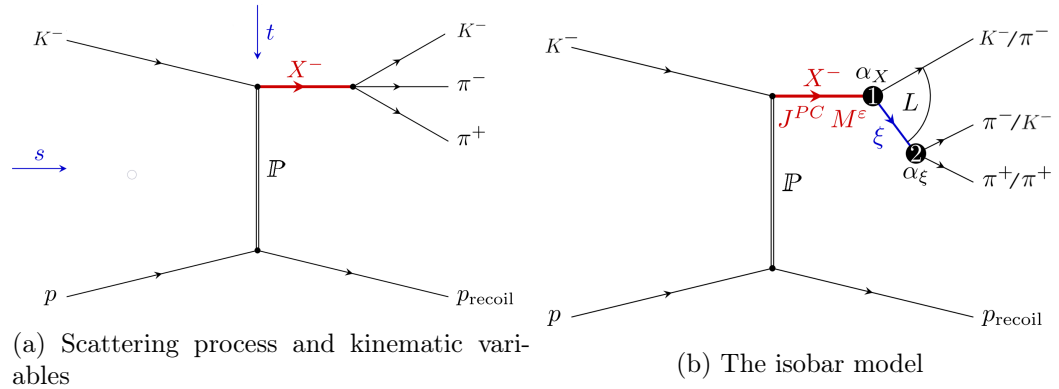

(a) Scattering process and kinematic variables

(b) The isobar model

Figure 1.1: An overview of the scattering process $K^- + p \rightarrow K^- \pi^+ \pi^- + p_{\text{recoil}}$

production amplitude $\mathcal{T}$, describing the production of the intermediate state X, and a *decay amplitude* Ψ, describing the decay of X into the three-body final state:

$$\mathcal{M}_{f,i} = \mathcal{T}(m_X, t') \cdot \Psi(m_X, \tau) \tag{1.3}$$

The kinematic distribution of the final-state particles depends only on the invariant mass m_X, the reduced squared four momentum transfer $t' \equiv |t| - |t|_{\min}$, $|t|_{\min}$ being the minimum value of $|t|$ needed to produce an intermediate state with $m_X > m_{K^-}$, and a set of five kinematic variables τ needed to describe the three-body system.

1.1.2 Isobar model

To describe the decay of X into the final-state particles K^-, π^+ and π^-, it is convenient to use the isobar model, illustrated in fig. 1.1b. In this model, the decay is described as a chain of subsequent two-body decays via additional intermediate two-body resonances, the *isobars* ξ, i.e.

$$X \to \xi + 1 \quad \text{and} \quad \xi \to 2 + 3 \tag{1.4}$$

Particle 1 is called the bachelor particle. Note that in our case, there are two possibilities for the isobar subsystem: it could consist of a $K^-\pi^+$ state or a $\pi^-\pi^+$ state. We also neglect final state interactions by assuming that the outgoing particles do not interact with each other. In the first decay, an orbital angular momentum L between the final-state particle 1 and the isobar ξ may arise. The decay amplitude $\Psi(m_X, \tau)$ describes the entire kinematics of the final state for particular X quantum numbers, orbital angular momentum L and the isobar ξ.

1.1.3 Reference frames and kinematic variables

The two decays in eq. (1.4) are described in specific reference frames, by boosting into the rest systems of the X and the isobar ξ, respectively.

The Gottfried-Jackson frame is used to describe the decay of the intermediate state X, which is at rest in this reference frame. Since the outgoing particles are emitted back-to-back, the angular distribution can be described by the polar angle ϑ_{GJ} and the azimuthal angle ϕ_{GJ} of one of the daughter particles.

The isobar decay is described in the so-called helicity frame. Again, the two final-state particles are emitted back-to-back, the angular distribution is hence given by the angles ϑ_{HF} and ϕ_{HF} of one outgoing particle.

Together with the isobar mass m_ξ, we obtain the five variables describing kinematic distribution of the final-state particles:

$$\tau \;=\; (\; m_\xi,\; \vartheta_{GJ},\; \phi_{GJ},\; \vartheta_{HF},\; \phi_{HF} \;) \tag{1.5}$$

1.1.4 Two-body decays

The two-body decays $R \rightarrow 1 + 2$ that are taking place in the discussed reference frames are represented by the two-body decay amplitudes $\mathcal{A}_{J_R, M_R}^R$, where J_R and M_R are the spin of R and its projection. This decay amplitude can be factorized into an angular and a dynamical part, while summing over the helicities of the daughter particles:

$$\mathcal{A}_{J_R, M_R}^R = \sum_{\lambda_1, \lambda_2} f_{\text{ang}}^{J_R, M_R}(\vartheta_R, \phi_R, \lambda_1, \lambda_2) \cdot f_{\text{dyn}}^{J_R, M_R}(m_R, \lambda_1, \lambda_2) \tag{1.6}$$

The angular part is given by first principles and completely defined by the quantum numbers of the particles. The dynamical part, however, describes the dependence of the amplitude on the invariant mass m_R of the subsystem and needs to be modeled. This will be discussed in section 1.4. The dynamical part also contains the usually unknown coupling α_R appearing at the decay vertex.

Using the isobar model, we can factorize the total decay amplitude Ψ into

$$\Psi(m_X, \tau) = \sum_{\lambda_\xi} \mathcal{A}_{J_X, M_X}^X(m_X, \vartheta_{GJ}, \phi_{GJ}) \cdot \mathcal{A}_{J_\xi, M_\xi}^\xi(m_\xi, \vartheta_{HF}, \phi_{HF}) \tag{1.7}$$

Here, the daughters K^-, π^+ and π^- are spin-0 particles, thus having helicities $\lambda_{K, \pi} = 0$. Hence, we sum only over the helicity $\lambda_\xi = \pm 1$ of the isobar .

1.1.5 Partial-wave decomposition

The amplitude Ψ for the decay $X \rightarrow K^- \pi^+ \pi^-$ is uniquely defined by two indices: the set $i = (I^G, J^{PC}, M)$ of the X quantum numbers and $j = (\xi, L)$, which represents a particular decay channel with isobar ξ and orbital angular momentum L. We therefore write $\Psi = \Psi_{i,j}$. This amplitude is often called *partial wave*, defined by its indices (i, j), which contain all information about the decay. Initially, the production amplitudes in eq. (1.3) depend only on the X quantum numbers. However, it is convenient to absorb the unknown couplings of the decay vertices α_X and α_ξ, which describe the strength and phase of the decay, into the unknown production amplitudes. This is done by redefining Ψ and $\mathcal{T}$:

$$\tilde{\Psi}_{i,j} = \frac{\Psi_{i,j}}{\alpha_X \alpha_\xi} \tag{1.8}$$

$$\tilde{\mathcal{T}}_{i,j} = \alpha_X \alpha_\xi \, \mathcal{T}_i \tag{1.9}$$

The modified production amplitudes are referred to as "transition amplitudes", since they now also contain information about the decay channel. The indices i and j represent a certain partial wave $a = (i, j)$. In order to obtain the total amplitude, we

sum coherently over all contributing partial waves. The measured intensity distribution is hence given by

$$\mathcal{I}(m_X, t', \tau) = \left| \sum_{a=i,j} \tilde{\mathcal{T}}_a(m_X, t') \cdot \tilde{\Psi}_a(m_X, \tau) \right|^2 + \mathcal{I}_{\text{flat}} \qquad (1.10)$$

Notice we have incoherently added the so-called *flat wave*. It is an isotropic phase-space distribution $\mathcal{I}_{\text{flat}} = |\mathcal{T}_{\text{flat}}|^2$ that models the contaminations from misreconstructed or only partially reconstructed events.

1.2 Binning of the data

The goal of the partial-wave analysis is to extract the unknown transition amplitudes $\{\mathcal{T}_a\}$ by fitting eq. (1.10) to the data.The transition amplitudes contain information about the X resonances. However, their dependence on the invariant mass m_X is a-priori unknown. Therefore, the event sample is divided into equidistant m_X bins that are narrower than the typical resonance widths. Also, the t' dependence of $\mathcal{T}_a$ is unknown. This is solved by further dividing the data into t' bins, in such way that each bin contains approximately the same number of events. Within a given (m_X, t') bin, we neglect the dependence on these two variables. That way, no assumption about the resonance content of the intermediate state X has to be made in the analysis process. Also, the intensity in a given kinematic cell is only a function of the phase-space variables τ, and the transition amplitudes appear in it as constants:

$$\mathcal{I}(\tau) = \left| \sum_a \tilde{\mathcal{T}}_a \cdot \tilde{\Psi}_a(\tau) \right|^2 + \mathcal{I}_{flat} \qquad (1.11)$$

Here, the sample is divided into 100 m_X bins. The total mass spectrum of the sample is 0.5 GeV/c^2 < m_X < 2.5 GeV/c^2. Each mass bin thus has a width of $\Delta m_X = 20$ MeV/c^2. The sample is also divided into eleven non-equidistant t' bins.

To simplify the notation, we will from now on refer to the redefined amplitudes $\tilde{\Psi}_a$ and $\tilde{\mathcal{T}}_a$ as Ψ_a and $\mathcal{T}_a$.

1.3 Maximum Likelihood method

The maximum likelihood method is a method to estimate the values of parameters of a model function by maximizing the *likelihood function* $\mathcal{L}$, which is the joint probability density of the dataset. For a dataset $\boldsymbol{x} = (x_1, ..., x_N)$ of N measurements that follow the same probability density function $f(\boldsymbol{x}; \boldsymbol{\theta})$ with m unknown

parameters $\boldsymbol{\theta} = (\theta_1, ..., \theta_m)$, and in the case where the number N of data points is not predetermined, the likelihood function is:

$$\mathcal{L}(\boldsymbol{\theta}, \lambda; \boldsymbol{x}, N) = \underbrace{\frac{\lambda^N e^{-\lambda}}{N!}}_{\substack{\text{Poisson} \\ \text{distribution}}} \underbrace{\prod_{k=1}^{N} f(x_k, \boldsymbol{\theta})}_{\substack{\text{Likelihood} \\ \text{function}}} \tag{1.12}$$

We apply the maximum likelihood method to our partial-wave analysis to estimate the values of the transition amplitudes $\{\mathcal{T}_a\}$ in our model for the intensity distribution $\mathcal{I}(\tau)$ in eq. (1.11). In this case, the likelihood function is given by

$$\mathcal{L}(\{\mathcal{T}_a\}) = \frac{\bar{N}^N}{N!} e^{-\bar{N}} \prod_{i=1}^{N} \underbrace{\frac{\mathcal{I}(\tau_i; \{\mathcal{T}_a\})}{\int d\varphi_3(\tau)\epsilon(\tau)\mathcal{I}(\tau; \{\mathcal{T}_a\})}}_{\text{probability for event } i} \tag{1.13}$$

Here, N is the number of measured events and $\bar{N}$ is the expected number of events measured by the detector. $\bar{N}$ depends on the *detector acceptance* $\epsilon(\tau_n)$, which corresponds to the probability of measuring an event produced at the phase-space coordinates τ_n:

$$\bar{N} = \int d\varphi_3(\tau)\epsilon(\tau)\mathcal{I}(\tau; \{\mathcal{T}_a\}) \tag{1.14}$$

To find the maximum likelihood estimate for the $\{\mathcal{T}_a\}$, we need to maximize the likelihood function in eq. (1.13). Since the value of $\mathcal{L}$ at the maximum is irrelevant, constant factors are omitted. To obtain a numerically better behaved expression, the logarithm of $\mathcal{L}$ is used . This yields

$$\begin{aligned}
\ln \mathcal{L} = \sum_{i=1}^{N} \log & \left(\left| \sum_a \mathcal{T}_a \Psi_a(\tau) \right|^2 + \mathcal{I}_{\text{flat}} \right) \\
& - \sum_{a,b} \mathcal{T}_a \mathcal{T}_b \underbrace{\int d\varphi_3(\tau)\epsilon(\tau)\Psi_a \Psi_b^*}_{\equiv I_{ab}} \\
& - \mathcal{I}_{\text{flat}} \underbrace{\int d\varphi_3(\tau)\epsilon(\tau)}_{\equiv I_{\text{flat}}}
\end{aligned} \tag{1.15}$$

The integral matrix I_{ab} is calculated using Monte Carlo methods. The transition amplitudes $\mathcal{T}_a(m_X, t')$ are determined by maximizing the likelihood function in eq. (1.15) independently in every (m_X, t') bin. Note that, as numerical methods traditionally find the minimum of a given function, we minimize the negative log-likelihood, $-\ln \mathcal{L}$, in practice.

1.4 Isobar parametrization

The choices of the isobar resonances, which contribute to the sum in eq. (1.11), and of the parametrization of their amplitudes which appear in eqs. (1.6) and (1.7), have a great influence on the result of the partial-wave analysis. They are therefore an important source of model dependence and hence systematic uncertainties.

As mentioned in section 1.1.2, two different isobar subsystems appear in our analysis. The isobar can either be constituted of a $K^-\pi^+$- or of a $\pi^-\pi^+$-system. These systems are dominated by certain isobar resonances. First, the appearance of the various possible isobar resonances depends on the invariant mass m_X. At lower m_X, isobar resonances with mass larger than $m_X - m_{\text{bachelor}}$ cannot be produced, or contribute only partially depending on their width. One must also take into account the total spin of the resonance: the higher the spin, the more the appearance of the resonance is suppressed. We therefore choose to include resonances with spin up to $J = 2$. Former experiments, e.g. [1], also hint which resonances dominate the two-body subsystems. For the scope of this thesis, we select the following isobar resonance ground states for our analysis:

Table 1.1: The four studied resonances

Name	Mass [MeV/c^2]	Width [MeV/c^2]	Strangeness S	Spin parity J^P
$\rho(770)$	769.0	150.9	0	1^-
$f_2(1270)$	1275.5	186.7	0	2^+
$K^*(892)$	895.81	47.4	$+1$	1^-
$K_2^*(1430)$	1432.4	109	$+1$	2^+

Although they contribute to the data, we did not include the $J^P = 0^+$ resonances, e.g. $f_0(500)$ for $\pi^-\pi^+$ and $K_0^*(700)$ for $K^-\pi^+$, since these resonances are very broad and the usual approximations and parametrizations discussed below cannot be applied, rendering them difficult to describe and analyse. As this thesis constitutes a proof of principle of the isobar parameter analysis method, we choose isobar resonances that are better known and approximately well-behaved.

As introduced in eq. (1.6), the two-body decay amplitude for the isobar decay is split up in an angular and a dynamical part. The latter one contains the dependence on the invariant mass m_ξ of the two-body subsystem:

$$f_{\text{dyn}}(m_\xi) = \mathcal{D}_\xi(m_\xi) \cdot F_{L_\xi}(m_\xi) \tag{1.16}$$

The dynamical amplitude consists of:

1. the angular-momentum barrier factor $F_{L_\xi}(m_\xi)$, which describe the centrifugal barrier effect caused by the orbital angular momentum L_ξ in the ξ decay

2. the propagator term $\mathcal{D}_\xi(m_\xi)$, which describes the propagation of the intermediate state ξ. It is equivalent to the line shape of ξ.

We need to make assumptions on the resonances ξ that appear as isobars and model their line shape. The isobar resonances are usually described by a relativistic Breit-Wigner amplitudes of the form:

$$\mathcal{D}_\xi^{\mathrm{BW}}(m_\xi; m_0, \Gamma_0) = \frac{1}{m_0^2 - m_\xi^2 - im_0\Gamma(m_\xi)} \tag{1.17}$$

with m_0 and Γ_0 being the nominal mass and width of the resonance. For narrow resonances, assuming that $\Gamma(m_\xi) = \Gamma_0$ is a good approximation. For wider resonances however, a mass-dependent width has to be used to accurately describe the opening of the phase-space over the resonance width.

Chapter 2

Method of determination of isobar parameters

2.1 Isobar parameter dependence

As we have seen in section 1.4, our isobar model and thus the whole partial-wave analysis result depends substantially on the isobar parameters. The propagator terms in eqs. (1.6), (1.7), (1.16) and (1.17) that describe the unstable isobars contain the masses and widths of the included isobar resonances as parameters. In order to calculate the decay amplitude, we therefore need to specify values for these masses and widths.

However, we cannot leave the isobar parameters as free parameters in the PWA fit. As seen in eq. (1.15), the likelihood function contains the integral matrix I_{ab} that is expensive to calculate. By ensuring that the decay amplitudes do not contain any free parameters, these amplitudes as well as the integral matrix I_{ab} can be pre-calculated before maximizing the likelihood function, rendering the whole computational process actually feasible in terms of computing time. The values for the masses and widths of the isobar resonances can therefore not be determined from data in the maximum-likelihood fit, but have to be specified beforehand.

These isobar parameter values are usually taken from the Particle Data Group (PDG) [2]. However, the mass and width values for the mesonic resonances are in some cases known only poorly. In addition, some of the parameters depend also on the experiment and the production channel. To take an example, the PDG lists the width of the $f_2(1270)$ resonance (neutrally produced) as $\Gamma = 186.7^{+2.2}_{-2.5}$ MeV. However, the experimental results vary between $\Gamma = 240 \pm 40$ and $\Gamma = 152 \pm 9$ MeV. This leads evidently to considerable systematic uncertainties, the studies of which is the goal of this thesis.

We will therefore study how well the PDG parameter values fit the COMPASS data based on the likelihood function in eq. (1.15). The presence of the bachelor particle may cause final-state interactions between the particles and non-resonant contributions might distort the line-shape of the isobars, leading to effective masses and widths values that differ from the PDG values.

2.2 Isobar parameter scans and likelihood maximum

2.2.1 Parameter range

In order to determine the optimal isobar parameters, we perform *parameter scans* for various isobar resonances; i.e. we carry out the partial-wave analysis process multiple times using various isobar resonance parameter values in a certain parameter range. This way, we obtain the values of the minimum of the negative log-likelihood generated for these isobar values. We select one isobar resonance to study and select a grid of parameter values, i.e. mass and width values, to be probed, relative to the

values from the PDG. Note that we vary the two parameters, isobar mass and width, independently and simultaneously, so that we perform a two-dimensional parameter scan. This is crucial for our analysis, since, as we will see in chapter 3, the optimal isobar parameter values are often shifted in mass and width compared to the PDG values. The parameter interval have to be adapted for each isobar resonance. Hence the parameter ranges may cover intervals from $\pm$ a few MeV to $\pm$ 50 MeV depending on the isobars and their behavior. The ranges are determined in such way that the log-likelihood difference between the parameter points is in the order of a few log-likelihood units.

2.2.2 Computational procedure

The parameter scans are basically done by handing over modified particle data values to the analysis program. After choosing the parameter range and number of steps, we perform the analysis process multiple times using the modified isobar parameter values. The procedure for a single scanning step is as follows: The decay amplitudes as well as the integrals discussed in sections 1.3 and 2.1 are pre-calculated. We then use the maximum-likelihood method to fit the intensity distribution model presented in eq. (1.10) to the measured data, by minimizing the negative log-likelihood in eq. (1.15). For this last step, we perform 50 fit attempts with random start values, in order to make sure the global $-\ln \mathcal{L}$ minimum is found.

2.2.3 Isobar parameter scans

Now that we have performed PWA fits using different isobar masses and widths within the chosen parameter range, we can associate with each set of isobar parameter values a maximum likelihood value, i.e. each fit can be represented by a point in the $(m, \Gamma, \mathcal{L})$ space. The complete scan for one isobar resonance then consists of numerous points within the mass and width range, each associated with a value of the maximum likelihood.

Since all performed PWA fits have the same number of free parameters (the transition amplitudes $\{\mathcal{T}_a\}$), the value of the maximum likelihood is a measure for the agreement of the model with the data. Obviously, our goal is to find those isobar parameter values that correspond to the highest likelihood value, and hence, fit best to the experimental data. We are also interested in the likelihood trend amongst the scan points. First of all, we have to make sure that the maximum we found is not at the borders of the chosen parameter range, as then, there could be parameters with a higher likelihood value. Also, the curvature around the likelihood maximum provides information about how well the maximum is localized (see section 2.2.5).

2.2.4 Graphical representation

It is easier and clearer to examine the results of the parameter scans by representing the data graphically in a three-dimensional plot like fig. 2.1. For each studied isobar resonance, we plot mass and width along the x- and y-axes and assign to each point a likelihood value along the z-axis. However, as discussed in section 1.3, we compute the negative log-likelihood $-\ln\mathcal{L}$. Therefore, we search for the *minimum* of the log-likelihood instead of for the maximum of $\mathcal{L}$. Moreover, the absolute log-likelihood value is irrelevant, we are only interested in the log-likelihood difference with respect to the minimum. The following plots, figs. 2.1 to 2.3, are results from scans with Monte Carlo data (see section 3.2), where the isobar parameters are known and correspond to the PDG values. These PDG resonance parameters are indicated by a dark-blue point.
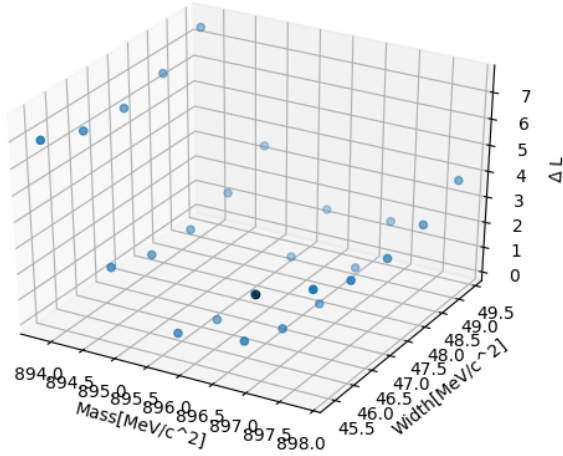

Figure 2.1: Result of a parameter scan for the $K^*(892)$-isobar with MC data

The maximal log-likelihood difference with respect to the minimum should be in the order of a few units to gain significant information. Indeed, due to the asymptotic normality of the likelihood function, $\mathcal{L}$ is a Gaussian in the parameters in the limit of an infinitely large data sample, meaning that $\ln\mathcal{L}$ is a parabola. Hence, in the vicinity of the minimum of the negative log-likelihood function, the scan points should follow a second-order surface. We can thus fit a two-dimensional parabola to the scan points, following the equation:

$$z(x,y) = a_1 \cdot x^2 + a_2 \cdot x + a_3 \cdot y^2 + a_4 \cdot y + a_5 \cdot x \cdot y + a_6 \tag{2.1}$$

Using a least-square approach, we can determine the parameters of the parabola. The parameters are used to determine the minimum of the parabola, thus finding the exact position of the negative log-likelihood minimum. We have now extracted the optimal isobar parameter values from our scan!

Figure 2.2 shows the fit of eq. (2.1) to the points in fig. 2.1. Here, the value of the parabola minimum is used to define the origin of the z-axis; i.e. the vertical position of the points is given by the log-likelihood difference from the computed minimum. This minimum is also represented by the red point in the graph.
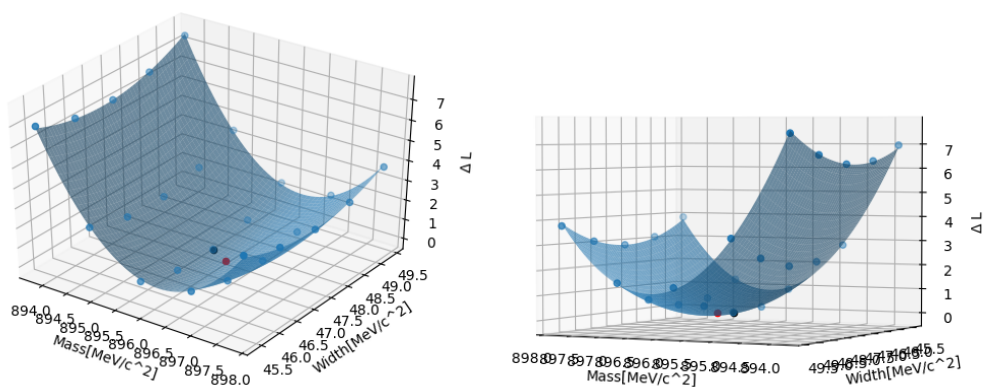

Figure 2.2: Like fig. 2.1, but with fitted parabola overlaid. The red point indicates the minimum of the parabola.

2.2.5 Uncertainty estimation

In addition to the best estimate for the isobar parameters, we can also calculate their uncertainties from the fitted parabola. This information is required to be able to compare the measured isobar parameter values to the unmodified parameter values and see if there is a discrepancy.

The curvature of the parabola at the minimum relates to the uncertainty of the isobar parameters. Indeed, the steeper the parabola is in the vicinity of its minimum, the smaller are the uncertainties. This is illustrated in figure 2.3: On the left, the result of a scan is shown based on a data sample with 5000 events; The diagram on the right shows the same for a 10 times larger data sample with 50 000 events. Because of the increased size of the data sample, the curvature of the fitted parabola is larger: while we use the same parameter values for the points of both scans, the log-likelihood difference on the scan with 50 000 events is way higher than on the 5000 events scan.

There are at least two ways to estimate the uncertainties of the isobar parameters.
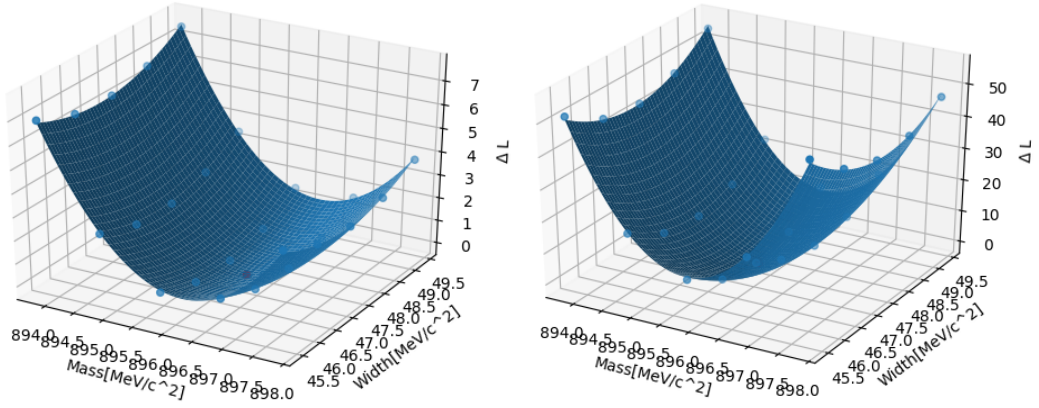
Figure 2.3: Scans of the $K^*(892)$ isobar resonance, using MC data samples of different size. Left: 5000 events; Right: 50 000 events.

First, there is a graphical method where the uncertainty ellipse in the (m, Γ) plane is determined by the intersection of the horizontal plane at $\Delta \mathcal{L} = 1/2$ with the second order surface.

Calculating the uncertainties numerically is, however, more convenient. To do so, we compute the uncertainties directly from the curvature of the parabola. An estimate to the covariance matrix $\hat{\boldsymbol{V}}$ of the isobar parameters is given by the negative inverse of the Hessian matrix $\hat{\boldsymbol{H}}$ of our parabolic curve at the maximum likelihood estimate

$$\hat{\boldsymbol{V}} = -\hat{\boldsymbol{H}}^{-1} \tag{2.2}$$

Hence, the standard deviations are given by the square root of the diagonal elements of the covariance matrix:

$$\Delta m = \sqrt{\left(-\hat{\boldsymbol{H}}^{-1}\right)_{11}} \tag{2.3}$$

$$\Delta \Gamma = \sqrt{\left(-\hat{\boldsymbol{H}}^{-1}\right)_{22}} \tag{2.4}$$

Chapter 3

Results and Discussion

In this chapter, we present the results of the parameter scans of the isobar resonances, for Monte Carlo data as well as for real data.

3.1 Data

We inspect data from two different invariant mass bins[1]:

$$m_X \in [1.30, 1.32] \text{ GeV}/c^2$$
$$m_X \in [1.80, 1.82] \text{ GeV}/c^2$$

The mass bin may influence on the result of the scan, especially for isobar resonances with masses m_ξ larger than m_X.

As introduced in section 1.4 and table 1.1, the four studied isobar resonances are the $\rho(770)$ and $f_2(1270)$ in the $\pi^-\pi^+$-subsystem and the $K^*(892)$ and $K_2^*(1430)$ resonances with strangeness $S = +1$ in the $K^-\pi^+$-subsystem.

For each isobar resonance, we perform a parameter scan in each m_X bin, as explained in chapter 2, using first Monte Carlo data and then real datasets. We compute the values of the log-likelihood minima for each set of isobar parameters and compare them to the unmodified parameter values. Assuming a parabolic dependence of the log-likelihood on the isobar parameters, we perform a fit in order to extract the isobar parameters that correspond to the global minimum of the negative log-likelihood. The goodness of the fit is also interesting, as it gives us an indication on the validity of our parabolic assumption.

Note that while we change the parameters for one isobar resonance, the parameters of other isobar resonances remain unchanged. Therefore, this approach does not take into account possible correlations between the parameters of different isobars.

3.2 Monte Carlo analysis

Before studying the real data, the analysis method was verified using generated pseudo-data with known values of the isobar parameters. For this task, isotropic phase-space events were generated using Monte Carlo methods[1] and weighted according to the intensity in eq. (1.11). This is done the following way: For each phase-space event, the decay amplitudes $\Psi_a(\tau)$ are calculated. For the transition amplitudes $\mathcal{T}_a$, we use prior fit results[1] from real data. With these amplitudes, the intensity $\mathcal{I}(\tau)$ can be computed for every phase-space event. The calculated intensity

---

[1]The real and Monte Carlo data, as well as the transition amplitudes $\mathcal{T}_a$ have been provided by [3]

is applied as a weight using the acceptance-rejection-method. The parameter scans are then performed on these Monte Carlo data.

The Monte Carlo (MC) data are generated (according to the intensity distribution model $\mathcal{I}(\tau)$) using the Particle Data Group values for the isobar resonance parameters. The scan results should be consistent with the values of the isobar parameters that we used to generate the MC data. Once this is verified for each inspected isobar resonance, the real data can be analysed.

3.2.1 MC study in the 1.80 GeV/c^2 mass bin

We begin with isobar parameter scans in the $m_X = 1.80$ GeV/c^2 mass bin.

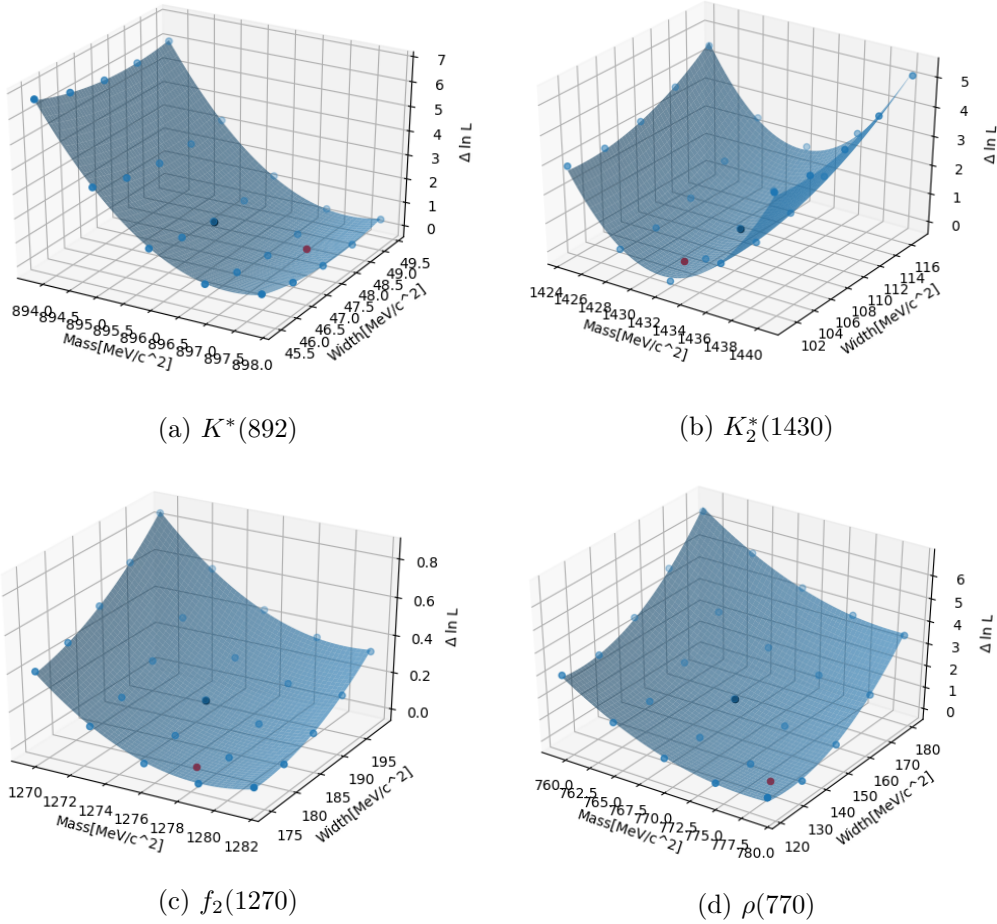(a) $K^*(892)$

(b) $K_2^*(1430)$

(c) $f_2(1270)$

(d) $\rho(770)$

Figure 3.1: Like fig. 2.2, but for the scan of the resonance parameters using MC data, for the 1.8 GeV/c^2 mass bin.

The results of the MC scans of the four studied isobar resonances are shown in fig. 3.1. The results are listed in table 3.1. The positions of the parabola minima are within the uncertainties compatible to the unmodified PDG parameter values which were used to generate the MC data.

Resonance	Mass at minimum [MeV/c^2]	PDG mass [MeV/c^2]	Width at minimum [MeV/c^2]	PDG width [MeV/c^2]
$K^*(892)$	897.2 ± 1.0	895.8	48.0 ± 2.1	47.4
$K_2^*(1430)$	1431.8 ± 3.1	1432.4	103 ± 8	109
$f_2(1270)$	1279 ± 11	1275.5	174 ± 30	186.7
$\rho(770)$	777 ± 8	769.0	130 ± 19	150.9

Table 3.1: Isobar parameter values from the study of MC data in the $m_X = 1.8$ GeV/c^2 bin

3.2.2 MC study in the 1.30 GeV/c^2 mass bin

We repeat the parameter scans for the Monte Carlo data in the 1.30 GeV/c^2 m_X bin. The scans are shown in fig. 3.2, and the results are presented in table 3.2. For the two isobars with lower masses, $K^*(892)$ and $\rho(770)$, the scan results resemble those from the 1.80 GeV/c^2 mass bin, and the parameter values that correspond to the shown negative log-likelihood minimum are consistent with the PDG parameter values within the uncertainty estimates.

For the $f_2(1270)$ and $K_2^*(1430)$ isobars, however, the parameter scans yield nothing useful. As discussed in section 1.4, at low m_X, not all resonances appear as isobars. Both the $f_2(1270)$ and the $K_2^*(1430)$ have masses that are larger than $m_X - m_{\text{bachelor}}$. Hence, only their low-mass tails, which are nearly independent of the resonance parameters, may contribute to the data. This is confirmed by the isobar parameter scans: the log-likelihood difference across the studied isobar parameter range is extremely small and we cannot fit a parabola to the scan points. We therefore conclude that the parameters of these two isobar resonances have no influence on our model in this m_X range.

3.3 Real data analysis

Now that we have shown that the method works on MC data, we can study the model dependence of the PWA result on the isobar parameters using real data. The goal is to investigate if there are any discrepancies between the isobar parameters that correspond to the lowest negative log-likelihood value and the PDG parameter values for each isobar resonance that are used in the standard PWA fit, i.e. if we can
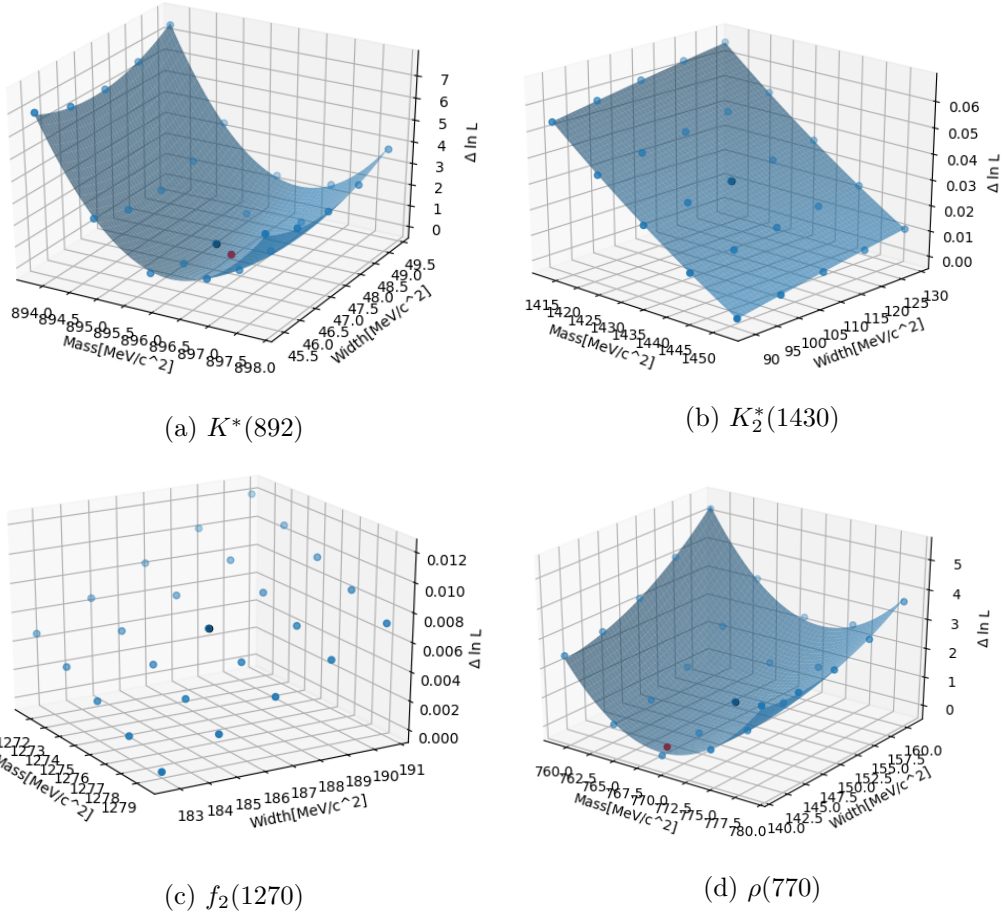
(a) $K^*(892)$

(b) $K_2^*(1430)$

(c) $f_2(1270)$

(d) $\rho(770)$

Figure 3.2: Like fig. 2.2, but for the scan of the resonance parameters using MC data, for the 1.3 GeV/c^2 mass bin.

find isobar parameter values for our model that make it fit better to the measured data. We thus perform parameter scans of the four isobar resonances and in both m_X bins. In sections 3.3.1 and 3.3.2, the results for $K^*(892)$, $K_2^*(1430)$ and $f_2(1270)$ will be presented. The $\rho(770)$ isobar will be treated separately in section 3.3.3.

3.3.1 Real data study in the 1.80 GeV/c^2 mass bin

In this section, we present the results of the parameter scans for the $K^*(892)$, $K_2^*(1430)$ and $f_2(1270)$ isobar resonances in the 1.80 GeV/c^2 m_X bin. The three scans are shown in fig. 3.3 and the numerical results are presented in table 3.3. The scans resemble those using Monte Carlo data. While the differences between the

Resonance	Mass at minimum [MeV/c^2]	PDG mass [MeV/c^2]	Width at minimum [MeV/c^2]	PDG width [MeV/c^2]
$K^*(892)$	896.2 ± 0.7	895.8	47.2 ± 1.4	47.4
$K_2^*(1430)$	none found	1432.4	none found	109
$f_2(1270)$	none found	1275.5	none found	186.7
$\rho(770)$	770 ± 5	769.0	142 ± 9	150.9

Table 3.2: Isobar parameter values for the study of MC data in the $m_X = 1.3$ GeV/c^2 bin

isobar parameters at the negative log-likelihood minima and the PDG parameter values is relatively large for some isobars, especially for the $f_2(1270)$, the large uncertainties make them compatible. The estimated isobar parameter values match the PDG values within one to two standard deviations. For the three isobars, the second-order surfaces fit the scan points well.

Resonance	Mass at minimum [MeV/c^2]	PDG mass [MeV/c^2]	Width at minimum [MeV/c^2]	PDG width [MeV/c^2]
$K^*(892)$	896.9 ± 1.5	895.8 ± 0.20	52.0 ± 3.3	47.4 ± 0.5
$K_2^*(1430)$	1427 ± 5	1432.4 ± 1.3	104 ± 10	109 ± 5
$f_2(1270)$	1283 ± 15	1275.5 ± 0.8	216 ± 38	$186.7^{+2.2}_{-2.5}$

Table 3.3: Isobar parameter values of real data parameter scans in the $m_X = 1.8$ GeV/c^2 bin

3.3.2 Real data study in the 1.30 GeV/c^2 mass bin

We are now going to present the results of the parameter scans for the $K^*(892)$, $K_2^*(1430)$ and $f_2(1270)$ resonances in the 1.30 GeV/c^2 m_X bin. The scans are shown in fig. 3.4, and the parameter values found are listed in table 3.4. The scan of the $K^*(892)$ isobar resonance parameters is similar to the scan in the 1.80 GeV/c^2 m_X bin. The parameters of the minimum match the PDG values within the uncertainties, although the $K^*(892)$ width deviates nearly 2.5 times the standard deviation. For the $K_2^*(1430)$ and $f_2(1270)$ resonances, however, no minimum in the negative log-likelihood can be found. This coincides with the observations made in the Monte Carlo analysis in section 3.2.2. In the 1.3 GeV/c^2 m_X bin, only the low-mass tail of these two resonances contributes to the data. Hence, there is no significant log-likelihood change across the parameter range.
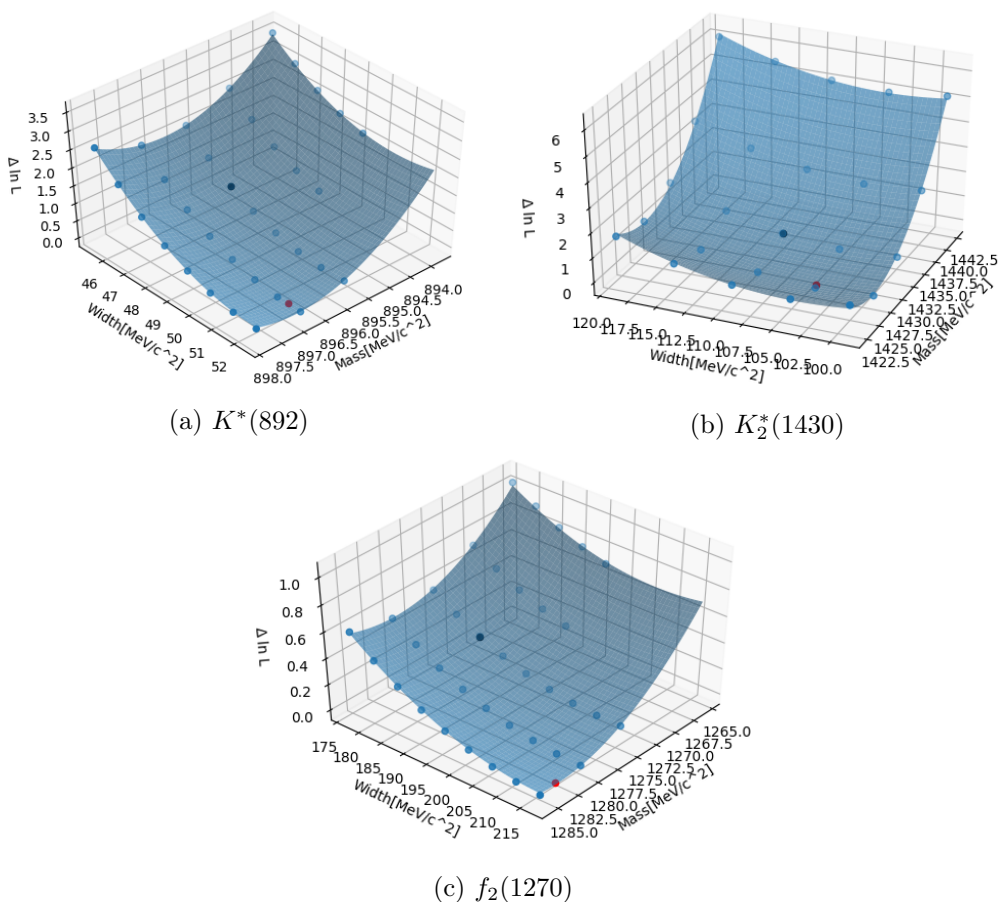
(a) $K^*(892)$

(b) $K_2^*(1430)$

(c) $f_2(1270)$

Figure 3.3: Like fig. 2.2, but for the resonance parameter scans of three resonances using real data for the $m_X = 1.8$ GeV/c^2 mass bin.

3.3.3 Real data study of the $\rho(770)$ isobar resonance

For the $\rho(770)$ isobar, the scans reveal major discrepancies between the parameter values of the negative log-likelihood minimum and the PDG values in both m_X bins. The scan plots are shown in fig. 3.5, and the numerical results are summarized in table 3.5.

The PDG lists the mass and width of the $\rho(770)$ resonance as $m_{\text{PDG}} = 769.0 \pm 0.9$ MeV/c^2 and $\Gamma_{\text{PDG}} = 150.9 \pm 1.7$ MeV/c^2. The mass of the negative log-likelihood minimum of the scans differs only slightly from the PDG value in the 1.3 GeV/c^2 m_X bin. In the 1.8 GeV/c^2 bin, the estimated mass is a little more than two standard deviations away from the PDG value. The $\rho(770)$ widths at the negative log-likelihood minima, however differ significantly from the PDG value. In the 1.8 GeV/c^2 m_X

(a) $K^*(892)$

(b) $K_2^*(1430)$

(c) $f_2(1270)$
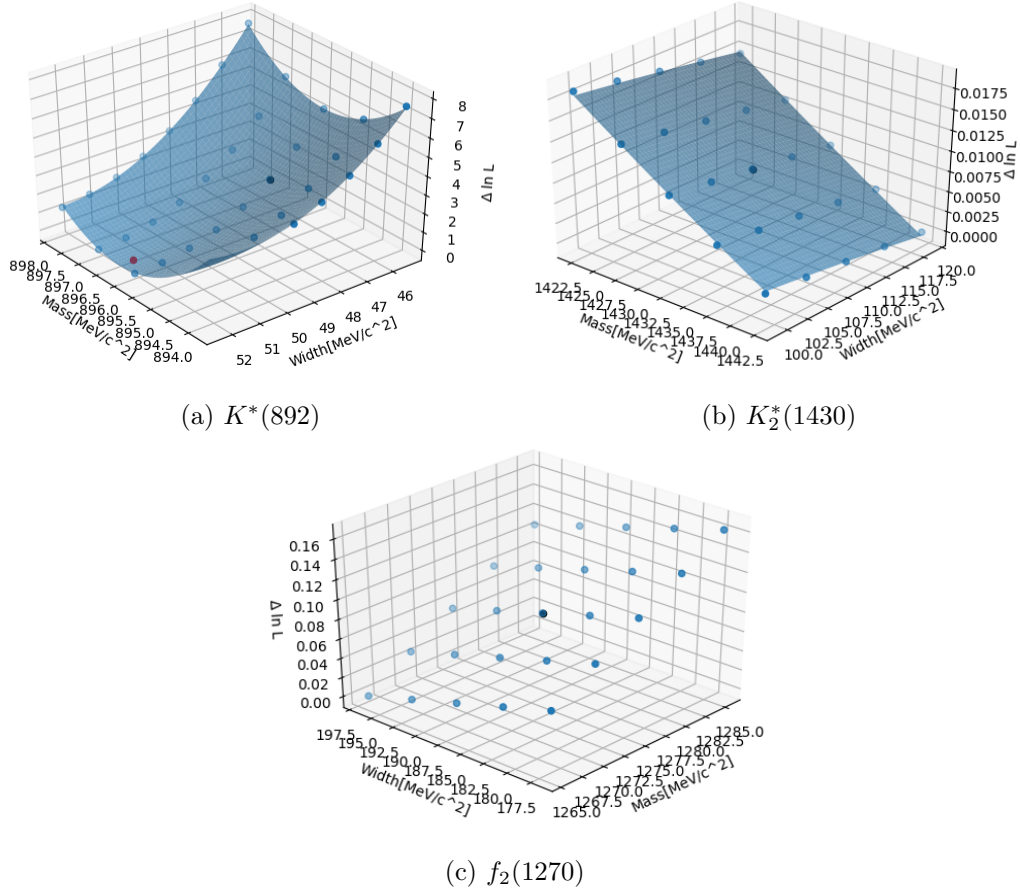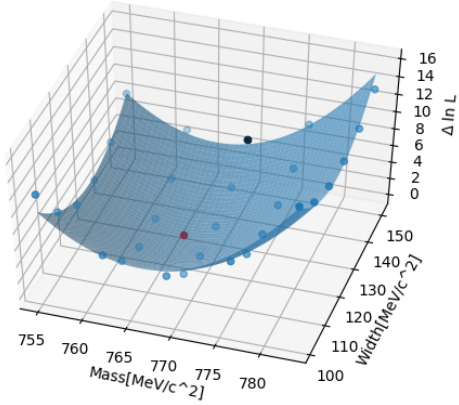
Figure 3.4: Like fig. 2.2, but for the resonance parameter scans of three resonances using real data for the $m_X = 1.3$ GeV/c^2 mass bin.

bin, the negative log-likelihood minimum is located at $\Gamma_{\min} = 94 \pm 12.8$ MeV/c^2, which is more than 4.4 σ away from the PDG value. This difference is still present, although less pronounced, in the 1.3 GeV/c^2 m_X bin, where the width deviates by approximately 2.8 σ.

The scan points also do not fit well the parabolic assumption that we make at the negative log-likelihood minimum. This is shown in fig. 3.6, where we see the parabolas and scan points from the side. There are significant vertical mismatches between scan points and the parabolas especially in the 1.3 GeV/c^2 m_X bin. We can calculate a pseudo-χ^2 coefficient by adding together the vertical differences squared and dividing by the amount of data points. In the 1.3 GeV/c^2 m_X bin, this yields $\chi^2 = 0.466$, and in the 1.8 GeV/c^2 m_X bin, we get $\chi^2 = 0.053$. To put those

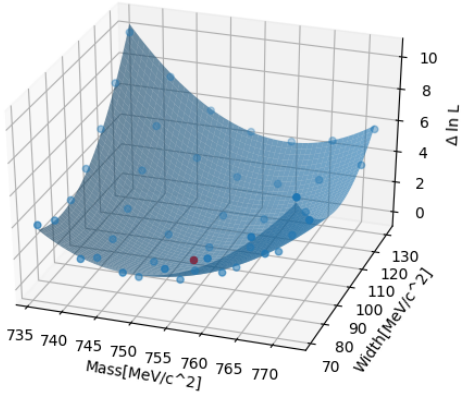| Resonance	Mass at minimum [MeV/c^2]	PDG mass [MeV/c^2]	Width at minimum [MeV/c^2]	PDG width [MeV/c^2]
$K^*(892)$	896.2 ± 1.0	895.8 ± 0.20	51.9 ± 2.0	47.4 ± 0.5
$K_2^*(1430)$	none found	1432.4 ± 1.3	none found	109 ± 5
$f_2(1270)$	none found	1275.5 ± 0.8	none found	$186.7^{+2.2}_{2.5}$

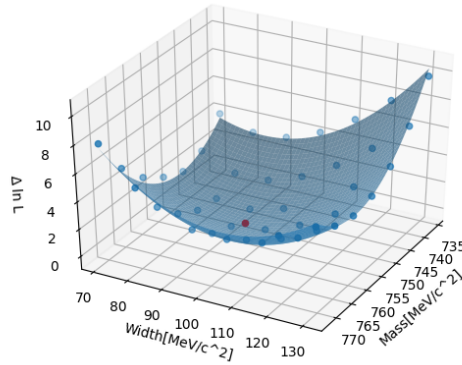Table 3.4: Isobar parameter values of real data parameter scans in the $m_X = 1.3$ GeV/c^2 bin

(a) $\rho(770)$, 1.30 GeV/c^2 mass bin
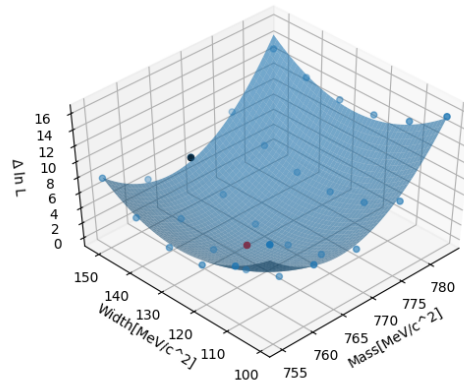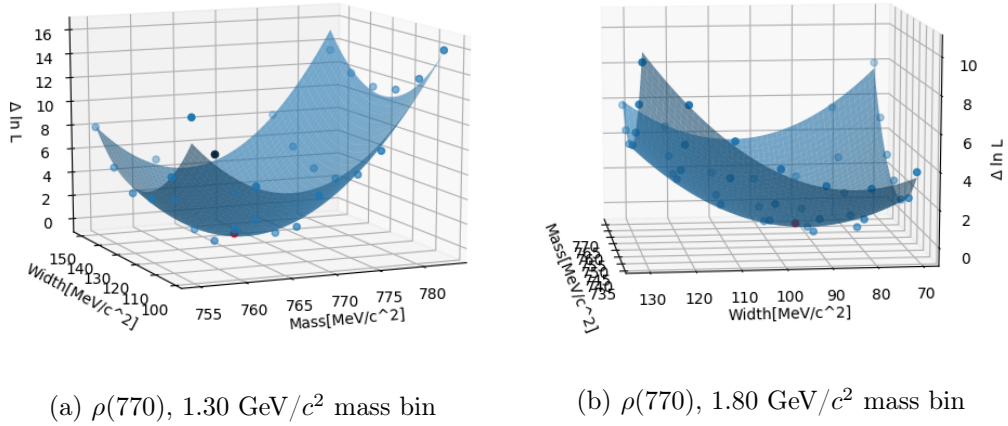
(b) $\rho(770)$, 1.30 GeV/c^2 mass bin

(c) $\rho(770)$, 1.80 GeV/c^2 mass bin

(d) $\rho(770)$, 1.80 GeV/c^2 mass bin

Figure 3.5: Like fig. 2.2, but for the real data $\rho(770)$ parameter scans in both mass bins.

m_X bin [GeV/c^2]	Mass at minimum [MeV/c^2]	Width at minimum [MeV/c^2]
[1.30, 1.32]	766 ± 4	128 ± 8
[1.80, 1.82]	753 ± 7	94 ± 13
PDG values (MeV/c^2):	769.0 ± 0.9	150.9 ± 1.7

Table 3.5: Parameter values for the $\rho(770)$ isobar

(a) $\rho(770)$, 1.30 GeV/c^2 mass bin

(b) $\rho(770)$, 1.80 GeV/c^2 mass bin

Figure 3.6: Like fig. 2.2, only showing the $\rho(770)$ isobar parameter scans with the fitted parabola from the side.

numbers into perspective, we can calculate the χ^2 coefficient for, e.g., the parabolic fit of the $K^*(892)$ isobar parameter scan in the 1.3 GeV/c^2 m_X bin, which yields $\chi^2 = 0.00106$.

We thus have considerable discrepancies of the $\rho(770)$ parameters between the negative log-likelihood minimum and the PDG values and gaps between the parabola and the scan points, indicating our parabolic assumption comes to its limits. Effects of final-state interactions between the three outgoing particles K^-, π^+, π^- are expected to shift the parameter values. However, these effects should be smaller than the differences we observe for the $\rho(770)$ width. Thus, even though final-state interactions may appear, an additional phenomenon has to cause the observed discrepancies. One possible cause could be systematic effects in the analysis. Indeed, some partial-waves appearing in the $\rho(770)$ isobar are hard to distinguish. The modification of the $\rho(770)$ parameters may induce alterations of the partial-wave intensities: intensity could be transferred from partial waves to others, which could cause the observed effects.

3.4 Recapitulation

For the three isobar resonances $K^*(892)$, $K_2^*(1430)$ and $f_2(1270)$, no significant disagreements between the estimated optimal parameter values and the model values could be found. Minor differences could be caused by final-state interactions. For the $\rho(770)$ resonance however, new optimal parameters have been determined that are significantly different from the PDG values. These deviations and the low quality of our parabolic fit cannot be simply explained by final-state interactions.

Chapter 4

Conclusion and Outlook

The partial-wave analysis of the $K^-\pi^+\pi^-$ data from the COMPASS experiment is performed to identify and study hadronic resonances. The isobar model is used to calculate the amplitudes for the decays of the intermediate resonances into the $K^-\pi^+\pi^-$ final state. The model assumes that the decay proceeds in a series of subsequent two-body decays with an intermediate isobar state. This model, however, is largely dependent on the parameters of the isobar resonances, which constitutes a source for systematic uncertainties. The isobar resonances are usually modelled using Breit-Wigner amplitudes, where the masses and widths of the resonances have to be taken from other experiments.

We have conducted isobar parameter scans by selecting a particular isobar resonance to study and by performing PWA fits using modified isobar mass and width values arranged on a grid. The minimum log-likelihood value of each PWA fit is an indicator of how well the chosen parameter values fit the data. A complete scan for one isobar resonance consists of several points within the chosen mass and width range, each associated with a negative log-likelihood value. Using these scans, we estimate the optimal parameter values by fitting a second-order surface to our scan points and by computing the parabola minimum. The uncertainties are estimated from the curvature of the second-order surface. We then compare the estimated isobar parameters with the PDG world averages.

We have inspected four isobar resonances with spin-parity $J = 1^-$ and 2^+: $K^*(892)$, $\rho(770)$ and $K_2^*(1430)$, $f_2(1270)$. While the scans of the $K^*(892)$, $K_2^*(1430)$ and $f_2(1270)$ resonances yield optimal isobar parameter values that are in agreement with the PDG world averages, we observe significant disparities of the parameter values for the $\rho(770)$ isobar, ranging up to 50 MeV/c^2. These differences could be in part due to final-state interactions of the outgoing particles. In addition, the mixing of intensities of partial waves with the $\rho(770)$ isobar might play a role..

Further steps could be taken to continue the analysis of the $\rho(770)$ resonance parameters and to potentially find the source of the discrepancy. First, the partial-wave mixing hypothesis could be tested by studying the partial-wave intensities as a function of isobar parameters. Potential effects from correlations of the parameters of different isobar resonances could be studied by scanning through the parameters of several isobar resonances simultaneously. Such an approach is, however, practically limited to up to three isobars, since higher-dimensional analyses become increasingly costly.

Bibliography

[1] C. Adolph et al. »Resonance Production and $\pi\pi$ S wave in $\pi^- + p \to \pi^- \pi^- \pi^- + p_{\mathrm{recoil}}$ at 190 GeV/c«. In: *Physical Review D* 95.032004 (2017). arXiv: `1509.00992`.

[2] *Particle Data Group.* URL: `http://pdglive.lbl.gov/`.

[3] Stefan Wallner. PhD thesis in preparation.